JOURNAL OF SOLID STATE CHEMISTRY 74, 27–33 (1988)

New Oxyfluoride Compounds $TaFeNiO_4F_2$ and $TaVNiO_4F_2$

G. POURROY AND P. POIX

Département Sciences des Matériaux, EHICS, 1, rue Blaise Pascal BP 296, 67008 Strasbourg Cedex, France

AND J. P. SANCHEZ

Centre de Recherches Nucléaires, 67037 Strasbourg Cedex, France

Received May 8, 1987; in revised form October 14, 1987

New oxyfluoride of composition $TaFeNiO_4F_2$ and $TaVNiO_4F_2$ have been synthesized and investigated by X-ray diffraction, magnetic susceptibility, and ^{57}Fe Mössbauer spectroscopy. The iron compound crystallizes either with a rutile or an α-PbO_2 structure depending on the thermal treatment. The rutile structure only is observed for the vanadium compound. The rutile phases order (magnetically) at low temperatures. The Mössbauer data in the paramagnetic and ordered states confirm the chemical disorder between the Ta^{5+} and 3d transition metal ions.

Introduction

Many oxides or fluorides with a rutile structure have already been synthesized. In some of them, for example WV_2O_6 (*1*), WCr_2O_6 (*2*), $LiFe_2F_6$ (*3*), the cations are ordered along the *c* axis with the sequence *A–B–B–A*, so that the structure becomes trirutile. The magnetic cations (*B*), vanadium, chromium, or iron in our examples, are separated by diamagnetic ions (*A*), thus forming isolated magnetic dimers well above the tridimensional order temperature. These compounds are of great interest, because they permit a study of the magnetic behavior of low-dimensional systems. Indeed, the broad maximum of the WV_2O_6 and WCr_2O_6 magnetic susceptibilities has been shown to result from the antiferromagnetic coupling within isolated V(III)–V(III) or Cr(III)–Cr(III) dimers (*1*, *2*).

A trirutile order has not yet been observed in oxyfluoride rutile compounds, such as $NiMTiO_3F_3$ and $CoMTiO_3F_3$ (M = Fe, V), $VMTiO_4F_2$ (M = Ni, Co), or NiCo TiO_2F_4 (*4*). According to their rutile structure, the cationic sites (2a) are statistically occupied. This property may result from a difference between the oxidation states of the metals that was too small (II, III, IV) and/or cationic sizes that were too close. Indeed, the trirutile compounds so far known present a great difference in the cationic sizes (Li and Fe) or in the electrostatic charges (W(VI) and V(III)).

These observations prompted us to investigate the solid solutions between the two rutile phases $TaFeO_4$ ($TaVO_4$) and NiF_2. A cationic ordering is expected to be favored in these solid solutions owing to the largely different oxidation states and ionic radii of the cations.

In the following, we report the preparation, crystallographic structure, and results

0022-4596/88 $3.00

of magnetic susceptibility and Mössbauer measurements of two new oxyfluoride compounds $TaFeNiO_4F_2$ and $TaVNiO_4F_2$.

Preparation

NiF_2 powder, as a starting material, has been obtained by a new synthesis route; its preparation will be described first.

NiF_2

Nickel hydroxycarbonate powder is dissolved in HF giving a green dark solution which is dried. The yellow powder obtained is heated at 600°C under vacuum. The NiO formed is eliminated with HCl.

Anal. (*5*) Calcd: Ni, 60.71%; F, 39.29%. Found: Ni, 59.51%; F, 39.34%.

The quality of the NiF_2 powder was checked by X-ray diffraction and susceptibility measurements. The lattice parameters of the rutile cell ($a = 4.646 \pm 0.005$ Å, $c = 3.085 \pm 0.005$ Å) as well as the magnetic results ($T_N = 73.1$ K) are in good agreement with the published data (*6, 7*).

$TaFeNiO_4F_2$–$TaVNiO_4F_2$

The starting products Ta_2O_5 and Fe_2O_3 of purity greater than 99.9% are first dried. V_2O_3 is obtained by reduction of V_2O_5 under hydrogen atmosphere at 600°C during 1 day; the reduction is completely achieved at 1050°C. Ta_2O_5, Fe_2O_3 (V_2O_3), and NiF_2 are mixed in a stoichiometric ratio and ground. The mixture introduced in gold cylindrical crucibles is heated in an inconel tube under a purified argon atmosphere. Each compound has been subjected to two different thermal treatments described in Table I.

Anal. (*5*) Calcd for $TaFeNiO_4F_2$: Ta, 45.5%; Fe, 14%; Ni, 14.8%; F, 9.5%. Found: Ta, 44.4%; Fe, 13.65%; Ni, 14.3%; F, 10.1%.
Anal. (*5*) Calcd for $TaVNiO_4F_2$: Ta, 46%; V, 12.9%; Ni, 15%; F, 9.6%. Found: Ta, 45.85%; V, 12.9%; Ni, 14.7%; F, 9.3%.

X-ray fluorescence spectra taken before and after the heat treatment confirm these analyses (*8*).

Crystal Structure

X-ray powder diffraction patterns of Ta $FeNiO_4F_2$ and $TaVNiO_4F_2$ have been taken using a Kristalloflex Siemens diffractometer and cobalt radiation, $CoK\alpha_1 = 1.78901$ Å. Both samples A crystallized in the rutile structure (space group, $P4_2/mnm$) with the cationic site occupied statistically by the

TABLE I

CHARACTERISTICS OF THE $TaFeNiO_4F_2$ AND $TaVNiO_4F_2$ SAMPLES: THERMAL TREATMENTS, STRUCTURES, AND COLORS

	$TaFeNiO_4F_2$		$TaVNiO_4F_2$	
	A	B	A	B
First heating	650°C-3 days	650°C-3 days	700°C-3 days	700°C-3 days
Second heating		550°C-3 days		550°C-3 days
Structure	Rutile	Rutile + α-PbO_2	Rutile	Rutile
Color	Yellow brown		Black	

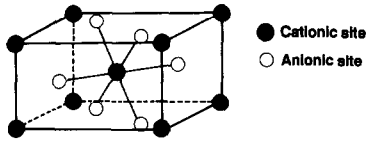

FIG. 1. Schematic representation of the rutile cell.

three metals (Fig. 1). Table II shows that their unit cell parameters are similar to the one observed for $TaFeO_4$ and $TaVO_4$ but larger than those found in the oxyfluorides with titanium (*4*). It should be noticed that the c/a ratios are almost constant ($0.647 < c/a < 0.661$) although Ta increases the lattice parameters (*4*). The lattice spacings and the corresponding intensities are listed in Tables IIIa and IIIb. The latter have been computed assuming a statistical occupation of the metallic sites and a mean positional parameter x for the anions. A distinction between the anionic sites has not been taken into account since it does not modify the intensities to a great extent. The two first diffraction lines have been eliminated owing to the X-ray absorption at low angles. The highest R value corresponds to the vanadium compound because the vanadium absorption adds to the tantalum one. The smallest reliability factor,

$$R = \sum |I_{calc} - I_{obs}| \Big/ \sum I_{obs},$$

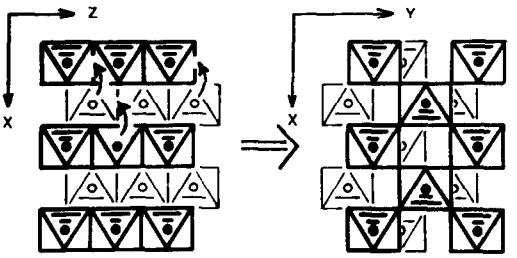

FIG. 2. Comparison of the rutile structure (left) with the α-PbO_2 structure type (right). Arrows indicate the possible cation movements for the transformation rutile $\rightarrow$ α-PbO_2. After Galy and Anderson (*10*).

has been obtained with $x = 0.299$ ($R = 6.5\%$) and $x = 0.302$ ($R = 7.8\%$) for the iron and vanadium compounds, respectively.

A trirutile structure, with a rearrangement along the c axis, has not been observed; instead, a α-PbO_2 structure (space group, *Pbcn*) appears for $TaFeNiO_4F_2$. Both the α-PbO_2 and rutile structures are built up from oxygen octahedra surrounding the metal atoms and bound together in strings through the structure by sharing edges and corners (*9*). A simple mechanism for the transformation rutile $\rightarrow$ α-PbO_2 has been proposed by Anderson and Galy (*10*); 50% of the cations are shifted in the way indicated by the curved arrows in Fig. 2. The difference in their structure is that in rutile these strings of octahedra are straight in the c axis because they share opposite

TABLE II

CRYSTALLOGRAPHIC PARAMETERS AND VOLUME CELLS OF $TaFeNiO_4F_2$ AND $TaVNiO_4F_2$ COMPARED WITH THOSE OF $TaFeO_4$ AND $TaVO_4$

	$TaFeNiO_4F_2$		$TaVNiO_4F_2$	TaFeO	$TaVO_4$
	Rutile	α-PbO_2	rutile	rutile (*11*)	rutile (*12*)
a	4.670 ± 0.01 Å	4.653 ± 0.01 Å	4.666 ± 0.01 Å	4.682 Å	4.667 Å
b		5.515 ± 0.01 Å			
c	3.045 ± 0.01 Å	5.057 ± 0.01 Å	3.046 ± 0.01 Å	3.048 Å	3.043 Å
c/a	0.652		0.652	0.651	0.652
V	66.408 Å^3	64.884 Å^3	66.316 Å^3	66.816 Å^3	66.28 Å^3

TABLE III

OBSERVED AND CALCULATED LATTICE SPACINGS AND INTENSITIES FOR $TaFeNiO_4F_2$ (a) AND $TaVNiO_4F_2$ (b)

a					b				
hkl	d_{obs}	d_{calc}	I_{obs}	I_{calc}	*hkl*	d_{obs}	d_{calc}	I_{obs}	I_{calc}
110*	3.296	3.302	149	184	110*	3.296	3.299	145	173
101*	2.549	2.551	114.0	132	101*	2.549	2.551	113	124
200	2.334	2.335	27.6	33	200	2.332	2.333	23.6	32
111	2.239	2.239	12.8	10	111	2.238	2.238	12.0	9.5
210	2.087	2.088	4.0	3	210	2.086	2.087	3.0	3
211	1.723	1.722	100	100	211	1.721	1.721	100	100
220	1.652	1.651	29	26	220	1.650	1.650	26.7	25.6
002	1.523	1.523	10	11	002	1.523	1.523	12.2	11
310	1.478	1.477	25	21	310	1.476	1.476	23	21.6
112	1.385	1.383	53	46.6	112	1.385	1.383	57.6	51.2
301		1.386			301		1.385		
311		1.329	0	0	311		1.328	0	0
202	1.277	1.275	10	9.4	202	1.276	1.275	12	10.2
212		1.230	0	0	212		1.230	0	0
321	1.194	1.192	20.5	17	321	1.192	1.191	18.2	18.8
400	1.169	1.168	7	6.3	400	1.167	1.167	6.4	6.8
410		1.133	0	0	410		1.132	0	0
222	1.121	1.120	16	13	222	1.120	1.119	22	14.7
330	1.1025	1.101	7	6.3	330	1.102	1.100	6.4	7.3
312	1.062	1.060	47	35.7	312	1.061	1.060	47	41.3
411		1.062			411		1.061		
420	1.046	1.044	9	8.5	420	1.043	1.043	9.4	10.3

Note. The asterisks indicate the reflections left out for the computation of the R values.

sides with each other, but in α-PbO_2, they are staggered along the a axis. It should be pointed out that monophasic $TaFeNiO_4F_2$ with α-PbO_2 structure was never obtained.

Let us note the strong contraction of the α-PbO_2 cell compared to the rutile one. A similar variation of the volume was also observed when comparing the compounds MTa_2O_6 and MNb_2O_6 (M = Fe, Co, Ni) of trirutile and columbite (ordered α-PbO_2) structures, respectively (*6*).

Bulk Magnetic Properties

The magnetic measurements have been performed with a pendulum-type magnetometer in the temperature range 4.2–300 K for the vanadium compound which is paramagnetic at room temperature. A Foner-type magnetometer was employed for the rutile iron compound which presents a field-dependent magnetization $\sigma = \sigma_0 + \chi H$. The ferromagnetic component σ_0 amounts to 0.17 uem/g at room temperature.

The inverse susceptibility curves versus temperature are presented in Figs. 3 and 4. The raw values are corrected from the diamagnetism calculated according to the SLATER and ANGUS method (*13*) (TaFe NiO_4F_2, -111.24×10^{-6} emu/mole; TaV NiO_4F_2, -111.07×10^{-6} emu/mole).

–Above 150 K, the susceptibilities follow Curie–Weiss laws:

$TaFeNiO_4F_2$, χ(emu/mole) = $4.70/(T + 250)$

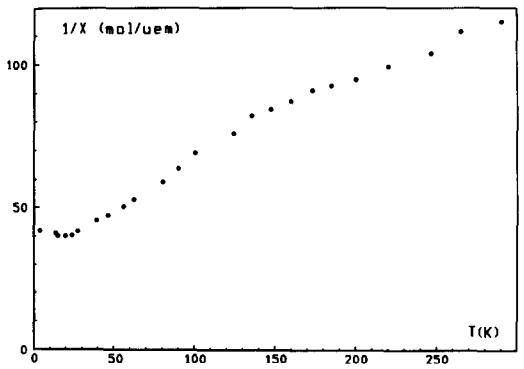

FIG. 3. Inverse susceptibility of $TaFeNiO_4F_2$ versus temperature.

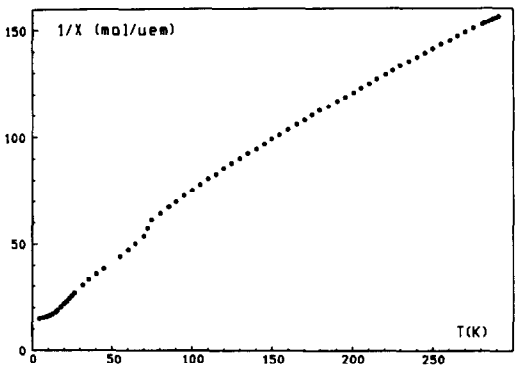

FIG. 4. Inverse susceptibility of $TaVNiO_4F_2$ versus temperature.

$TaVNiO_4F_2$, χ(emu/mole) = 2.59/(T + 114).

–$TaFeNiO_4F_2$ and $TaVNiO_4F_2$ present a maximum at 20 and 4 K, respectively.

Mössbauer Spectroscopy in $TaFeNiO_4F_2$

The ^{57}Fe Mössbauer spectra of $TaFeNiO_4F_2$, taken at 300, 77, and 4.2 K, were recorded using conventional mechanical drives synchronized with a multichannel analyzer operating in time mode. The ^{57}Co/Rh source was maintained at the same temperature as the absorber which contained about 3 mg/cm^2 of natural iron (the absorber thickness was chosen in order to minimize the high electronic absorption due to the heavy Ta ions). The Mössbauer spectra were computer analyzed as described in the text.

The ^{57}Fe Mössbauer data of the rutile $TaFeNiO_4F_2$ sample are presented in Table IV; the spectra are shown in Figure 5. At 300 and 77 K, the spectra present two main slightly asymmetric Mössbauer lines plus a weak resonance at about 2.4 mm/sec. Assuming Lorentzian line shapes, the spectra are satisfactorily analyzed as a superposition of two broadened quadrupole doublets indicating the presence of Fe^{3+} ions (~93%)

TABLE IV

MÖSSBAUER PARAMETERS OF THE Fe^{3+} IONS IN $TaFeNiO_4F_2$ (RUTILE) AT DIFFERENT TEMPERATURES

Temperature (K)	δ_{IS} (mm/sec) rel. Fe at RT	ΔEQ (mm/sec)	H_{hf} (kOe)	W (mm/sec)
300	0.41(1)	0.81(1)		0.53(1)
77	0.50(1)	0.83(1)		0.56(1)
4.2	0.53(2)	−0.10(1)[a]	473(2)	1.06(5) Outer 0.79(4) Middle 0.72(3) Inner

Note. δ_{IS}, isomer shift; ΔEQ, quadrupole splitting; H_{hf}, hyperfine field; W, linewidth.

[a] Effective quadrupole splitting (measured difference of the two outer lines to the right and the difference of the two outer lines to the left).

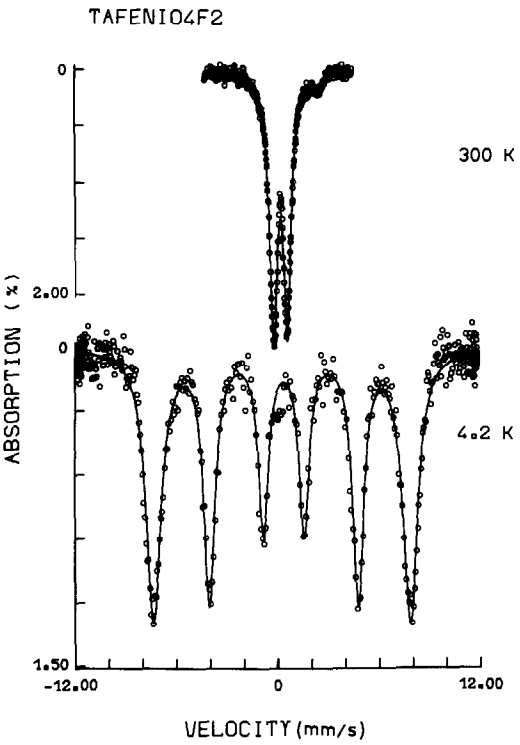

FIG. 5. ^{57}Fe Mössbauer spectra of $TaFeNiO_4F_2$ at 300 and 4.2 K.

and of a small amount of Fe^{2+} ions (~7%). The isomer shifts (δ_{IS}) and quadrupole splittings (ΔEQ) characterize iron ions in octahedral coordinations (Fe^{3+} ions see Table IV; Fe^{2+}, δ_{IS} = 1.16 mm/sec vs Fe, ΔEQ= 2.9 mm/sec at 300 K).

The Mössbauer spectrum recorded at 4.2 K (Fig. 5) shows that the iron ions experience a magnetic hyperfine field. The marked broadening of the outer lines compared to the middle and inner lines of the sextuplet characterizes a hyperfine field distribution estimated to be about ±20 kOe around the average value of 473 kOe.

Discussion and Conclusions

The Mössbauer line broadenings observed in the paramagnetic as well as in the magnetically ordered state of $TaNiFeO_4F_2$ are due to fluctuations of the local environment of the Fe^{3+} ions. The Mössbauer data thus confirm the X-ray diffraction results, i.e., a random distribution of the cations in the rutile structure. The occurrence, in the Mössbauer spectra, of a small fraction of Fe^{2+} ions (not detected by chemical analysis) is tentatively attributed to a fluorine deficiency. Although it is not clear whether the small Fe^{2+} fraction occurs in a separate phase or in solid solution the former possibility could explain the observation of the ferromagnetic component. However, contamination of the $TaFeNiO_4F_2$ sample by some Fe_3O_4 impurities is ruled out from the magnetization and X-ray data. It seems more convincing to correlate the magnetization value to $NiFe_2O_4$ impurities which can appear when small quantities of TaF_5 are volatilized. The $NiFe_2O_4$ contamination level is estimated from the σ_0 value to be 0.35 mole%. It is concluded that $TaFeNiO_4F_2$ is nonstoichiometric; this can be the reason for the partial rutile → α-PbO_2 transformation observed for sample B (Table I).

We now examine the magnetic properties. At low temperatures, the two oxyfluorides present a maximum in the susceptibility curves at the same temperature range as Ta_2MO_6 (M = Co, Fe, V, Cr, Ni) (*15*), $TaFeO_4$ and $TaVO_4$ (*16, 17*). At first sight, their maximum can be attributed to a long-range antiferromagnetic order. But this may be questionable when referring to the properties of $TaFeO_4$. Indeed, $TaFeO_4$, which presents a partial cations ordering, exhibits a complex behavior with magnetic short-range behavior coexisting with spin glass behavior (*17*). Thus, at this stage of the study, the exact nature of the magnetically ordered state remains unknown. Actually, as the metallic sites are statistically occupied, the diamagnetic tantalum separate finite entities of magnetic cations (monomers, dimers, trimers, . . .) along the c axis and a short-range magnetic order may thus exist above the ordering temperature. Such a situation has already been encountered in WVO_4 rutile (*18*) where, at

low temperature, the susceptibility follows a Curie–Weiss law with a reduced Curie constant indicating short-range magnetic order. The same hypothesis may explain the high-temperature magnetic behavior of $TaFeNiO_4F_2$. Indeed, in the paramagnetic region, the Curie constant is weaker than expected ($c_{th} = 5.375$). Moreover, the Fe^{2+} fraction, deduced from the Mössbauer spectra, is too low to explain such a diminution. Nevertheless, a more precise description of the magnetic order in these two oxyfluorides would require Mössbauer (on ^{57}Fe enriched) samples and neutron diffraction studies in the temperature range of the magnetic susceptibility maximum.

Another point which must be clarified is the influence of the nonstoichiometry on the transformation rutile $\rightarrow$ α-PbO_2. Furthermore, the role played by the cations must be elucidated; indeed, the cations involved in the solid solutions seem to have a great importance since vanadium does not induce this transformation. The extension of this study to other oxyfluorides is underway.

Acknowledgments

The authors thank Prof. O. Evrard and R. Gerardin (UA040158 Vandoeuvre Pes Nancy) for supplying the X-ray powder diffraction patterns.

References

1. G. Pourroy, M. Drillon, L. Padel, and J. C. Bernier, *Physical B + C* **123,** 21 (1983).
2. M. Drillon, L. Padel, and J. C. Bernier, *J. Chem. Soc. Faraday Trans. 2* **76,** 1224 (1980).
3. J. Portier, A. Tressaud, R. de Pape, and P. Hagenmuller, *C. R. Acad. Sci. Paris,* **267,** 1711 (1968).
4. R. H. Odenthal, J. Grannec, J. M. Dance, J. Portier, and P. Hagenmuller, *J. Solid State Chem.* **9,** 120 (1974).
5. Service Central d'Analyse CNRS BP 22 69390 Vernaison.
6. R. W. G. Wyckoff, "Crystal Structures," 2nd ed., Vol. 1 (1963).
7. J. W. Stout and E. Catalano, *Phys. Rev.* **92,** 1575 (1953).
8. R. Heimburger, UA405 Fluorescence X, EHIC Strasbourg, private communication.
9. J. H. Sturdivant, *Z. Kristallogr.* **75,** 88 (1930).
10. J. Galy and S. Andersson, *J. Solid State Chem.* **3,** 525 (1971).
11. M. Grillet, Thèse 3e cycle Paris XI (1974).
12. H. Trarieux, J. C. Bernier, and A. Michel, *Ann. Chim.* **4,** 183 (1969).
13. J. C. Bernier and P. Poix, *Actual. Chim.* **2,** 7 (1978).
14. M. Takano and T. Takada, *Mater. Res. Bull.* **5,** 449 (1970).
15. J. C. Bernier, *C. R. Acad. Sci. Paris* **273,** 1166 (1971).
16. N. A. Fadeeva, R. P. Ozerov, V. P. Smirnov, V. A. Makarov, E. F. Makarov, V. A. Povitsky, N. A. K. Rjukova, and R. B. Zorin, *J. Phys. C* **32**(1), 503 (1971).
17. N. A. Christensen, T. Johansson, and B. Lebech, *J. Phys. C* **9**(13), 2601 (1976).
18. G. Pourroy, C. Hornick, L. Padel, P. Poix, and J. C. Bernier, *Nouv. J. Chim.* **8,** 669 (1984).